

Structural distortion induced Dzyaloshinskii-Moriya interaction in monolayer CrI₃ at van der Waals heterostructures

Hongxing Li* and Wei-Bing Zhang†

*Hunan Provincial Key Laboratory of Flexible Electronic Materials Genome Engineering,
School of Physics and Electronic Sciences, Changsha University of
Science and Technology, Changsha 410114, People's Republic of China*

Guanghai Zhou

*Department of Physics, Key Laboratory for Low-Dimensional
Quantum Structures and Quantum Control (Ministry of Education),
and Synergetic Innovation Center for Quantum Effects and Applications,
Hunan Normal University, Changsha 410081, People's Republic of China*

The van der Waals (vdW) magnetic heterostructures provide flexible ways to realize particular magnetic properties that possess both scientific and practical significance. Here, by first-principles calculation, we predict strong Dzyaloshinskii-Moriya interactions (DMIs) by constructing CrI₃/Metal vdW heterostructures. The underlying mechanisms are ascribed the large spin-orbital coupling (SOC) of the I atom and the structural distortion in CrI₃ layer caused by interlayer interaction. This is different from the traditional way that deposit magnetic films on substrate to generate DMI, wherein DMI is dominated by interlayer hybridization and large SOC of substrates. In addition, both Heisenberg exchange and magnetic anisotropy are modulated dramatically, such as Heisenberg exchange is nearly doubled on Au(111), and the out-of-plane magnetism is enhanced by 88% on Ir(111). Our work may provide a experimentally accessible strategy to induce DMI in vdW magnetic materials, which will be helpful to the design of spintronics devices.

I. INTRODUCTION

Magnetism is the fundament of many modern technologies, such as magnetic storage. It is an interesting research field for a long history, and new magnetic phenomena emerge continually [1]. Due to the Pauli exclusion principle, and spin-orbital coupling (SOC) in solid, several energy terms related to magnetism are developed, including exchange interaction, magnetic anisotropy, and so on, and the magnetic properties are determined by synergetic effects of these terms [2]. Since the magnetic energy terms are related to both atomic and electronic structures, by selecting elements and designing structures, particular magnetic properties can be achieved [3].

The magnetic interfaces are rather accessible artificial structures. In 2000, Heinze et al. [4] deposited Mn atomic monolayer on W(110) substrate, and a two-dimensional (2D) antiferromagnetic structure is revealed. In addition, because the inversion symmetry is broken in interface, Dzyaloshinskii-Moriya interaction (DMI) may arise. DMI is antisymmetric, and can result in nonlinear magnetic structure, such as Skyrmions [3]. Skyrmion is a kind of spin structure that is topologically protected and behaves like particles, and can be applied in data storage and logic technologies [5]. The Skyrmion lattice in 2D system is firstly realized by depositing monolayer Fe film on Ir(111) surface [6].

At present, the major strategy to generate DMI is depositing 3d magnetic atoms on heavy 5d nonmagnetic

metal surface. Along with the experimental progress, many theoretical works have been carried out to understanding the underlying mechanisms. Belabbes et al. [7] systematically study a series of 3d atoms on different 5d substrates. They found that the strength and chirality of DMI are determined by occupations of 3d orbital and the hybridization between 3d and 5d orbitals. Yang et al. [8] elaborate that, in Co/Pt interface, despite magnetic moments are located at Cr site, the DMI is contributed by heavy Pt atoms that adjacent to Co layer. These works indicate that 3d-5d hybridization and the large SOC of substrates play critical roles to generate DMI.

In 2017, intrinsic 2D ferromagnetic materials CrI₃ and Cr₂Ge₂Te₆ are discovered successfully [9, 10], opening a new chapter in the magnetic materials. CrI₃ layer is ferromagnetic with out-of-plane magnetism. Both the exchange interaction and magnetic anisotropy arise from Cr-I-Cr superexchange path in which I atom has large SOC strength [11, 12]. However, DMI is absent in CrI₃ layer because the inversion symmetry. How to induce DMI in CrI₃ and other 2D magnetic material is an interesting topic now. Liu et al. [13] and Behera et al. [14] theoretically induce DMI in CrI₃ layer by applying perpendicular electric field, but very large electric field is required. Xu et al. [15] substitute one I atom layer in CrI₃ by Br(Cl) to fabricate Cr(I, X)₃ Janus monolayer, strong DMI, as well as topological spin texture are predicted.

In this study, we overlay CrI₃ layer on the widely-used substrates Ir(111), Pt(111) and Au(111). Note that monolayer CrI₃ has been prepared on Au(111) successfully [16]. Surprisingly, strong DMI in CrI₃/Metal is predicted by first-principles calculations. The primary un-

* lihx@csust.edu.cn

† zhangwb@csust.edu.cn

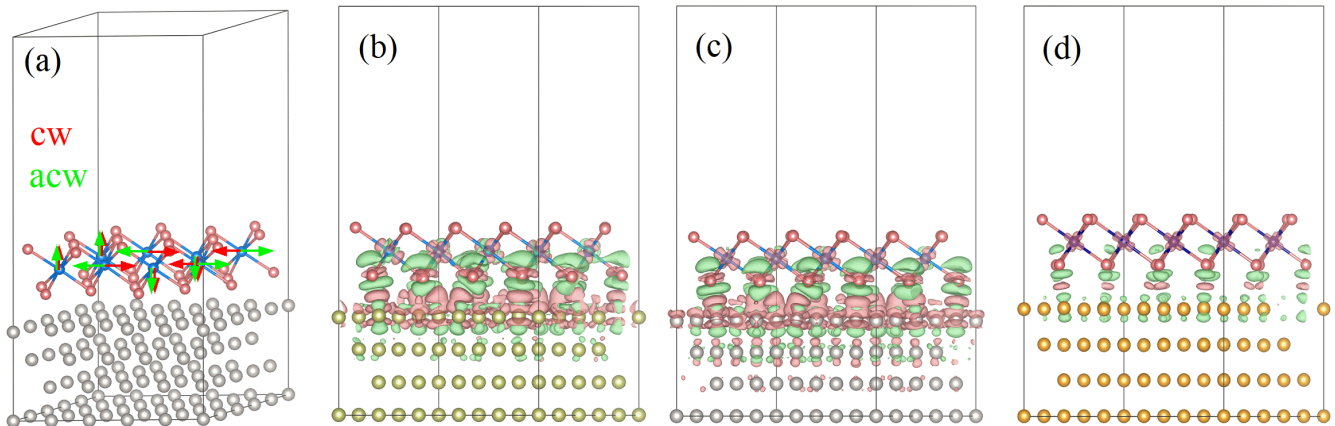


FIG. 1. (a) The structural schematic diagram of $\text{CrI}_3/\text{Metal}$. The red and green vectors indicate spin wave with opposite chirality. The interlayer charge density difference for (b) $\text{CrI}_3/\text{Ir}(111)$, (c) $\text{CrI}_3/\text{Pt}(111)$, and (d) $\text{CrI}_3/\text{Au}(111)$. Pink and light green represent charge accumulation and depletion, respectively. The isosurface is set to $0.002 \text{ e}/\text{\AA}^3$.

derlaying mechanisms are ascribed to the large SOC of I atom and structural distortion in CrI_3 layer induced by interlayer interactions. This is different from the conventional $3d/5d$ interfaces, in which the DMI is dominated by interlayer hybridization and large SOC of substrates. Our results will provide a guideline for the design of spintronics devices based on CrI_3 and other 2D magnetic materials.

II. CALCULATIONAL DETAILS

All our calculations are performed on Vienna ab initio simulation package (VASP) based on the framework of density functional theory [17, 18]. The interaction between electron and core is calculated by projected augmented wave (PAW) method [19]. The generalized gradient approximation (GGA) with Perdew-Burke-Ernzerhof (PBE) functional [20] is adapted to evaluate the energy exchange-correlation. An effective Hubbard value $U_{eff}=2 \text{ eV}$ is added to Cr $3d$ orbital within the scheme proposed by Dudarev et al. [21]. The cutoff energy of the plane-wave basis is set to 400 eV. Brillouin zone sampling is done by a $5 \times 5 \times 1$ Γ -center k-point mesh [22]. The convergence criteria for residual force and electronic step are $0.01 \text{ eV}/\text{\AA}$ and 10^{-5} eV , respectively. The DFT+D2 method is used to take the interlayer vdW force into account [23].

The heterostructures are constructed by overlaying CrI_3 2×2 supercell on Ir(111), Pt(111) and Au(111) 5×5 supercell with four atom layers, as shown in Fig. 1(a). During structural relaxation, the bottom atom layer of substrate is fixed to simulate the bulk condition. A vacuum slab of 15 \AA is added to avoid the artificial interaction between the periodic structures. The lattice constant of CrI_3 is optimized to be 7.01 \AA . To match the substrate, the CrI_3 monolayer should be compressed

(stretched) by -3.2% , -1.0% and 3.0% for Ir(111), Pt(111) and Au(111), respectively.

III. RESULTS AND DISCUSSIONS

After structural relaxation, the I atoms that face to substrates are pulled down, elongating the bottom Cr-I bonds. The average Cr-I bond length is summarized in Table I. We can find there is considerable difference between bottom and upper Cr-I bonds, and the largest value is 0.13 \AA in $\text{CrI}_3/\text{Ir}(111)$, indicating remarkable structural distortion in CrI_3 layer. This is different from the situation that putting CrI_3 onto 2D substrates, which the crystal undergoes negligible deformation [24–26]. To evaluate the interlayer interaction, adsorption energies E_{ad} are calculated by

$$E_{ad} = (E_{\text{CrI}_3} + E_{\text{Metal}} - E_{\text{CrI}_3/\text{Metal}})/m \quad (1)$$

where E_{CrI_3} , E_{Metal} and $E_{\text{CrI}_3/\text{Metal}}$ are the energy of CrI_3 layer, substrate and $\text{CrI}_3/\text{Metal}$ heterostructure, and m is number of unit cell of CrI_3 in $\text{CrI}_3/\text{Metal}$ with a value of 4. The results are 967, 752, and 400 meV for $\text{CrI}_3/\text{Ir}(111)$, $\text{CrI}_3/\text{Pt}(111)$, and $\text{CrI}_3/\text{Au}(111)$, respectively.

TABLE I. The calculated structural parameters for $\text{CrI}_3/\text{Metal}$ heterostructures.

	$\text{CrI}_3/\text{Ir}(111)$	$\text{CrI}_3/\text{Pt}(111)$	$\text{CrI}_3/\text{Au}(111)$
d (\AA)	2.67	2.61	3.05
Bottom Cr-I (\AA)	2.86	2.81	2.83
Upper Cr-I (\AA)	2.73	2.74	2.77
Δl (\AA)	0.13	0.07	0.06
E_{ad} (meV)	967	752	400

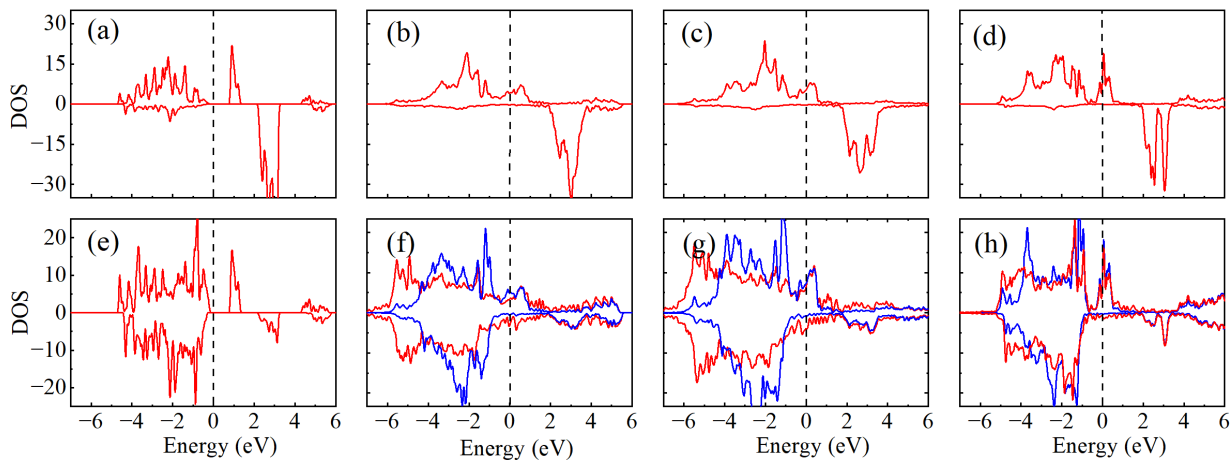


FIG. 2. The projected density states (PDOS) of Cr d and I p orbitals in CrI₃ layer. (a) (b) (c) and (d) The PDOS of Cr d orbital, (e) (f) (g) and (h) the PDOS of I p orbital for pristine CrI₃ monolayer, CrI₃/Ir(111), CrI₃/Pt(111) and CrI₃/Au(111), respectively. For PDOS of I atom, the red line and blue line represent the bottom and upper I atom layer, respectively.

The interactions between CrI₃ layer and substrates will lead to charge redistributions. We calculate the charge difference density (CDD) by

$$\Delta\rho = \rho_{Heter} - \rho_{Metal} - \rho_{CrI_3} \quad (2)$$

to further understand the interlayer interaction. The results that depicted in Fig. 1 show significant charge redistribution around interface, especially CrI₃/Ir(111) and CrI₃/Pt(111), indicating strong interlayer hybridizations. On the other hand, in accordance with relative small of E_{ad} , the charge redistribution in CrI₃/Au(111) is slight. The bottom I atoms in CrI₃ layer undergo great charge redistribution, while there is no obvious redistribution around the upper I atoms. Bader charge analysis [27] is used to understand the charge redistribution quantitatively. We find CrI₃ layer is hole-doped with 0.776 e by Pt(111), while it is electron-doped by Ir(111) and Au(111) with 0.032 e and 0.256 e, respectively. Interestingly, despite charge redistribution in CrI₃/Au(111) is weaker than CrI₃/Ir(111), there are more charge transfer in CrI₃/Au(111).

The average number of electrons at Cr atom, bottom and upper I atoms are summarized in Table II. In pristine CrI₃ layer, Cr atom is 4.687 e, and I atom is 7.438 e. Upon depositing on substrates, the amount of electrons accumulated at Cr atom range from 0.049 e to 0.138 e. On the other hand, the electrons of I atoms that face to substrates always decrease, but the upper I atom get slight electrons for all the cases.

To explore the effects of interlayer interactions on the electronic structure of CrI₃ layer, we plot the atomic projected density of states (PDOS) in Fig. 2. For comparison, we also depict the DOS of pristine CrI₃ layer in Fig. 2(a) and (b). The Cr³⁺ in pristine CrI₃ is in high spin states with 3 μ_B magnetic moments for three electrons occupy at spin-up t_{2g} orbitals [11]. Different from the semiconductive character of pristine CrI₃, there

are considerable states around Fermi level, thus CrI₃ layer undergoes metallization at interface. It should be noted that the spin splitting Cr d bands in CrI₃/Au(111) is about twice as large as the pristine CrI₃, indicating large magnetic stability. In the case of electronic states of I atoms in CrI₃/Ir(111) and CrI₃/Pt(111), the occupied states of bottom I atom delocalizes in a wider energy range than upper one. On the other hand, due to the weak interlayer hybridization in CrI₃/Au(111), the PDOS of bottom and upper I atoms are still similar.

Considering the remarkable alterations in atomic and electronic structures for CrI₃ layer in CrI₃/Metal, significant modulation in magnetic properties by interfacial effects can be expected. CrI₃ monolayer is a well understood ferromagnet with out-of-plane magnetization. The magnetic moment (MM) of Cr atom in pristine CrI₃ monolayer with ferromagnetic (FM) state is 3.116 μ_B . However, the MM increases markedly when CrI₃ layer is overlaid on substrates, since there are extra charges accumulate at Cr site and occupy spin-up states. On the other hand, the proximity induced MMs in substrates are several hundredth μ_B , which are about one order smaller than the MMs polarized by 3d magnetic atom layer [7]. This fact indicates the little orbitals overlap between Cr atom and substrate. This is different to 3d/5d interfaces, where 3d magnetic atoms interact with substrates

TABLE II. The interlayer charge transfer Δe from substrates to CrI₃ layer, and number of electrons occupied at Cr and I atoms. The unit is e.

	CrI ₃	Cr ₃ /Ir(111)	Cr ₃ /Pt(111)	CrI ₃ /Au(111)
Δe	0	0.032	-0.776	0.256
Cr	4.687	4.825	4.793	4.736
Bottom I	7.438	7.300	7.264	7.386
Upper I	7.438	7.480	7.475	7.460

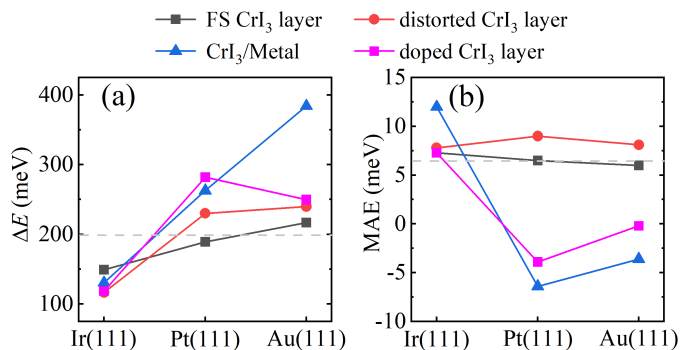


FIG. 3. The calculated exchange energy ΔE (a) and magnetic anisotropy energy MAE (b) for FS CrI₃ layer (blank), CrI₃ layer taken from CrI₃/Metal (red), CrI₃/Metal (blue) and charge doped CrI₃ layer (pink). The horizontal dash line represent the value of pristine CrI₃ layer.

directly, and then polarizes the substrates to large extent.

The strength of Heisenberg exchange interaction can be evaluated by the exchange energy, namely the total energy difference between Néel antiferromagnetic (AFM) and FM states, $\Delta E = E_{AFM} - E_{FM}$. Magnetic anisotropy energy MAE is calculated by $MAE = E_x - E_z$, in which the E_z (E_x) is total energy of the systems with out-of-plane (in-plane) magnetization in FM state. The results are plotted by red in Fig. 3. We find the ΔE increase by 32% and 93% in CrI₃/Pt(111) and CrI₃/Au(111), respectively, while CrI₃/Ir(111) has a small ΔE decreased by 34%. Although the negative effect on ΔE , Ir(111) enhance the out-of-plane MAE from 6.4 meV for pristine CrI₃ monolayer to 12.0 meV. However, Pt(111) and Au(111) flip magnetism direction to in-plane.

Interfaces can result in several effects, including strain, interlayer hybridization and charge transfer. Understanding how is the magnetism influenced by these interfacial effects is important to the design of magnetic heterostructures. To achieve this target, we further perform magnetism calculations to the freestanding (FS) CrI₃ layer with the lattice constants that match to substrates, distorted CrI₃ layer taken from the relaxed heterostructures, and the distorted CrI₃ layer doped with charge as the charge transfer in the corresponding CrI₃/Metal. The results are shown by different colour in Fig. 3. For FS CrI₃ layer, the magnetism is modulated by lattice constant (strain). We can see that the ΔE increase with lattice constant, but a contrary tendency to MAE. This is consistent with the previous studies about the tuning of magnetism of CrI₃ layer by strain [28, 29]. The distorted CrI₃ layer further suffers structural distortions resulted by interlayer interactions. Interestingly, MAE is always enhanced by structural deformations, owing to the reduced crystal symmetry [30]. The ΔE of CrI₃ layer taken from CrI₃/Pt(111) and CrI₃/Au(111) are larger than the corresponding FS CrI₃ layer, while a reduction of ΔE is caused by the crystal deformation in CrI₃/Ir(111).

We can understand this discrepancy from a geometrical perspective. Upon structural relaxation, the change of upper Cr-I-Cr bond angle is negligible, but the bottom one becomes small for all the systems. Nevertheless, in CrI₃/Pt(111) (CrI₃/Au(111)), the bond angle change from 93.4° (97.0°) to 89.2° (94.2°), respectively, which are more close to the ferromagnetic criterion of 90° from GKA rule for superexchange [31]. Conversely, the bond angle decreases from 91.4° to 84.6° by Ir(111), deviating largely from the ferromagnetic criterion. As a result, the ferromagnetism of Cr-I-Cr path is strengthened by Pt(111) and Au(111), while weakened by Ir(111).

Then we further dope the distorted CrI₃ layer by the corresponding interlayer charge transfer. Because the charge transfer in CrI₃/Ir(111) is very small, the doping effect on ΔE and MAE is tiny. Meanwhile, the ferromagnetism is enhanced by both hole and electron doping, the same as previous studies [26, 32]. Interestingly, the ΔE of charge doped CrI₃ layer is much smaller than CrI₃/Au(111). Therefore, though the relative weak interlayer hybridization in CrI₃/Au(111), it plays dominant role to enhance the Heisenberg exchange interaction of CrI₃. By contrast, the ΔE of charge doped CrI₃ are close to CrI₃/Ir(111) and CrI₃/Pt(111), thus the strong interlayer hybridization between CrI₃ with Ir(111) and Pt(111) influence the Heisenberg exchange interaction slightly. On the other hand, the magnetism direction is flipped from out-of-plane to in-plane by both electron and hole doping. In addition, interlayer hybridization in CrI₃/Pt(111) and CrI₃/Au(111) can further stable the in-plane magnetism. Surprisingly, the magnetism direction maintains out-of-plane in CrI₃/Ir(111), and the MAE even increases by 88% to a value of 12.0 meV. The out-of-plane anisotropy is crucial to the application of low dimensional magnetism [5]. Hence, CrI₃/Ir(111) is a potential candidate to fabrication of information device.

Another important effect in interface is the inversion symmetry breaking. In magnetic systems, combining with large enough SOC, Dzyaloshinskii-Moriya interaction (DMI) may arise. DMI among magnetic pair takes the form as [33]

$$E_{DM} = -\mathbf{D}_{ij} \cdot (\mathbf{S}_i \times \mathbf{S}_j) \quad (3)$$

which is antisymmetric and breaks chiral symmetry, thus the spin waves with opposite chirality are no long degenerate. On this account, we construct two short period spin waves with clockwise (cw) and anticlockwise (acw) chirality by the constrained magnetism as implemented in VASP [8], and calculate the corresponding total energy E_{cw} and E_{acw} , then the total DMI energy can be expressed by

$$d^{tot} = (E_{acw} - E_{cw})/n \quad (4)$$

where $n=8$ is number of Cr atom in CrI₃/Metal. As shown in Fig. 4, CrI₃/Ir(111) has the largest d^{tot} of 1.5 meV, and decreases monotonously to 0.6 meV for CrI₃/Au(111). The strengths are comparable to the

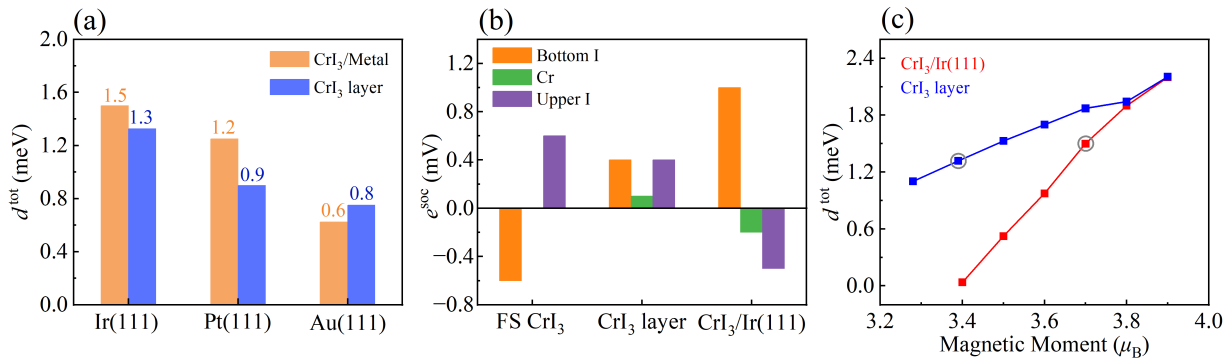


FIG. 4. (a) Total DMI of CrI₃/Metal and CrI₃ layer. (b) Atomic contribution to DMI. (c) DMI under different magnetic moments for CrI₃/Ir(111) and CrI₃ layer. The circled dots are the most energetically stable magnetic moments.

DMI in Janus [34] and FM/HM heterostructures, such as Co/Pt and Co/Ir [8]. Considering the out-of-plane magnetic anisotropy and weak Heisenberg exchange interaction, topological magnetic structure Skyrmions is likely to arise in CrI₃/Ir(111). On the other hand, vortex is possible in CrI₃/Pt(111) and CrI₃/Au(111) due to the in-plane magnetism. In $3d/5d$ interfaces, a similar trend of DMI for different substrates is also observed [7], and the magnitude of DMI for $3d$ atom layer deposited on Au(111) is always the smallest for the fulfilling $5d$ orbital and the subsequent weak $3d-5d$ orbital hybridization [7, 35]. However, as discussed above, in the vdW interfaces Cr atoms do not interact with substrates directly, the hybridization between Cr $3d$ and substrate $5d$ orbital should not be the key factor to generate DMI. To confirm this assumption, we calculate the DMI of distorted CrI₃ layer. The results show that CrI₃ layer also possesses sizable DMI that close to the interfaces, and the value is even greater CrI₃/Au(111). It should be noted that the MM of Cr atom in CrI₃/Metal is larger than CrI₃ layer. Consequently, we can conclude the structural distortion in CrI₃ layer caused by substrates take the major responsibility for the DMI in CrI₃/Metal. This is different from $3d/5d$ interfaces, in which the $3d-5d$ orbital hybridization is the crucial mechanism [7, 8, 36]. The results manifest that we can induce DMI in 2D magnetic materials by choosing substrates with appropriate activity which can result in structural distortion, instead of the substrate with large SOC to provide spin-orbit center.

The DMI is rooted in the variation of atomic SOC energy at different spin configurations. To clarify atomic contribution to DMI, taking CrI₃/Ir(111) as an illustrating example, we calculate the atomic resolved SOC energies difference e^{soc} for opposite chirality spin waves, and the results are depicted in Fig. 4(b). In FS CrI₃, the e^{soc} of Cr atom is zero, and upper and bottom I atom layers have same absolute values but opposite signs. This result is expectant because FS CrI₃ is inversion symmetric and the DMI must be zero. As to distorted CrI₃ layer taken from relaxed CrI₃/Ir(111), the results show crys-

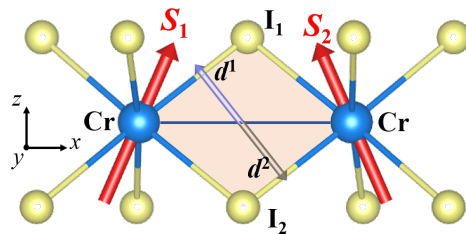


FIG. 5. Schematic show of DMI in CrI₃ layer.

tal distortion not only alters the magnitudes of e^{soc} , but also reverses the sign of bottom I atom. In addition, the e^{soc} for Cr atom layer is no long zero with the magnitude about 0.2 meV, because the octahedral ligand field of Cr atom is distorted and the orbital moment is no long totally quenched. Consequently, a non-zero DMI is generated and contributed mainly by heavy I atoms. This is similar to the situation in Janus [34, 37]. Interestingly, once CrI₃ layer hybridizes with substrate, despite d^{tot} of CrI₃ layer and CrI₃/Ir(111) are close, e^{soc} alters dramatically. The e^{soc} of bottom I atom layer is more than doubled, while Cr and upper I atom change to negative sign. In addition, we should point out that the e^{soc} of substrates in all the systems is negligible. The heavy atoms with strong SOC is crucial to DMI since they act as spin-orbital scattering [38]. However, in CrI₃/Metal, the Cr atom hybridize very weakly with substrates, so the superexchange path Cr- $5d$ atom-Cr does not develop. As a consequence, the contribution of substrates to DMI is tiny, even though strong SOC in substrates.

We further illustrate the DMI in Fig. 5. Among Cr pair where are two superexchange paths Cr-I₁(I₂)-Cr, and each path will generate DMI $d^1(d^2)$. According to Moriya's rule, the direction of DMI is perpendicular the plane determined by the three atoms in path [33]. In FS CrI₃, the two paths are equal, so the d^1 and d^2 are opposite with the same magnitude, resulting in zero net

DMI. However, in interfaces, because the structural distortion and interlayer hybridization, the two paths are no longer equal and d^1 can not cancel with d^2 . We note that net DMI may be tilted and has in-plane and out-of-plane components. Nevertheless, the average contribution of out-of-plane component to total energy is zero, and the above calculation is the in-plane component [34].

As stated above, the MMs of Cr atom in CrI₃ layer and CrI₃/Metal are different. To illustrate the dependence of DMI on MM, we derive the DMI as a function of the MM in Cr atom by constraining its magnitude for CrI₃/Ir(111), and the results are shown in Fig. 4(c). Positive linear relationships are found for both CrI₃ layer and CrI₃/Ir(111), but the slope of CrI₃/Ir(111) is steeper than CrI₃ layer. This is different from Co/Pt interface, wherein DMI decreases even changes the sign along with the increasing of Co magnetic moment [39]. As expressed in eq. (3), when the MMs are the same, d^{tot} of CrI₃ layer is always greater than CrI₃/Ir(111). If \mathbf{D}_{ij} is a constant, the value of energy is in direct proportion to the square of MM (spin). However, the linear relationships indicate the magnitude of \mathbf{D}_{ij} is inversely proportional to the square root of MM.

IV. CONCLUSIONS

In summary, we have predicted large DMI in vdW magnetic heterostructures CrI₃/Metal. Our calculations and analysis indicate the underlying mechanisms are the large SOC of I atom and structural distortion in CrI₃ layer, which are different to the traditional magnetic heterostructures where the DMI is generated by interlayer hybridization and the large SOC of substrates. In addition, both the Heisenberg exchange interaction and magnetic anisotropy energy can be tuned dramatically by substrates. This work will be helpful to the research of CrI₃ and the design of information device, since it provides an experimentally accessible way to induce DMI in vdW magnetic materials.

Note added. During the preparation of our manuscript, Zhang et al.[40] report the DMI in CrI₃ on Au and Cu substrates, but they attribute the mechanism to inter-layer charge transfer and chemical interactions.

ACKNOWLEDGMENTS

This work was supported by the National Natural Science Foundation of China (Grant No. 11874092 and 12174100), the Fok Ying-Tong Education Foundation, China (Grant No. 161005), and the Natural Science Foundation for Distinguished Young Scholars of Hunan Province (Grant No. 2021JJ10039).

-
- [1] H. Kurebayashi, J. H. Garcia, S. Khan, J. Sinova, and S. Roche, Magnetism, symmetry and spin transport in van der waals layered systems, *Nat. Rev. Phys.* **4**, 150 (2022).
- [2] D. Khomskii, *Transition metal compounds* (Cambridge University Press, 2014).
- [3] F. Hellman, A. Hoffmann, Y. Tserkovnyak, G. S. D. Beach, E. E. Fullerton, C. Leighton, A. H. MacDonald, D. C. Ralph, D. A. Arena, H. A. Dürr, P. Fischer, J. Grollier, J. P. Heremans, T. Jungwirth, A. V. Kimel, B. Koopmans, I. N. Krivorotov, S. J. May, A. K. Petford-Long, J. M. Rondinelli, N. Samarth, I. K. Schuller, A. N. Slavin, M. D. Stiles, O. Tchernyshyov, A. Thiaville, and B. L. Zink, Interface-induced phenomena in magnetism, *Rev. Mod. Phys.* **89**, 025006 (2017).
- [4] S. Heinze, M. Bode, A. Kubetzka, O. Pietzsch, X. Nie, S. Blügel, and R. Wiesendanger, Real-space imaging of two-dimensional antiferromagnetism on the atomic scale, *Science* **288**, 1805 (2000).
- [5] A. Fert, N. Reyren, and V. Cros, Magnetic skyrmions: advances in physics and potential applications, *Nat. Rev. Mater.* **2**, 1 (2017).
- [6] S. Heinze, K. Von Bergmann, M. Menzel, J. Brede, A. Kubetzka, R. Wiesendanger, G. Bihlmayer, and S. Blügel, Spontaneous atomic-scale magnetic skyrmion lattice in two dimensions, *Nat. Phys.* **7**, 713 (2011).
- [7] A. Belabbes, G. Bihlmayer, F. Bechstedt, S. Blügel, and A. Manchon, Hund's rule-driven Dzyaloshinskii-Moriya interaction at $3d-5d$ interfaces, *Phys. Rev. Lett.* **117**, 247202 (2016).
- [8] H. Yang, A. Thiaville, S. Rohart, A. Fert, and M. Chshiev, Anatomy of Dzyaloshinskii-Moriya interaction at Co/Pt interfaces, *Phys. Rev. Lett.* **115**, 267210 (2015).
- [9] B. Huang, G. Clark, E. Navarro-Moratalla, D. R. Klein, R. Cheng, K. L. Seyler, D. Zhong, E. Schmidgall, M. A. McGuire, D. H. Cobden, *et al.*, Layer-dependent ferromagnetism in a van der Waals crystal down to the monolayer limit, *Nature* **546**, 270 (2017).
- [10] C. Gong, L. Li, Z. Li, H. Ji, A. Stern, Y. Xia, T. Cao, W. Bao, C. Wang, Y. Wang, *et al.*, Discovery of intrinsic ferromagnetism in two-dimensional van der waals crystals, *Nature* **546**, 265 (2017).
- [11] W.-B. Zhang, Q. Qu, P. Zhu, and C.-H. Lam, Robust intrinsic ferromagnetism and half semiconductivity in stable two-dimensional single-layer chromium trihalides, *J. Mater. Chem. C* **3**, 12457 (2015).
- [12] D.-H. Kim, K. Kim, K.-T. Ko, J. Seo, J. S. Kim, T.-H. Jang, Y. Kim, J.-Y. Kim, S.-W. Cheong, and J.-H. Park, Giant magnetic anisotropy induced by ligand LS coupling in layered Cr compounds, *Phys. Rev. Lett.* **122**, 207201 (2019).
- [13] J. Liu, M. Shi, J. Lu, and M. P. Anantram, Analysis of electrical-field-dependent dzyaloshinskii-moriya in-

- teraction and magnetocrystalline anisotropy in a two-dimensional ferromagnetic monolayer, *Phys. Rev. B* **97**, 054416 (2018).
- [14] A. K. Behera, S. Chowdhury, and S. R. Das, Magnetic skyrmions in atomic thin CrI_3 monolayer, *Appl. Phys. Lett.* **114**, 232402 (2019).
- [15] C. Xu, J. Feng, S. Prokhorenko, Y. Nahas, H. Xiang, and L. Bellaiche, Topological spin texture in Janus monolayers of the chromium trihalides $\text{Cr}(\text{I}, \text{X})_3$, *Phys. Rev. B* **101**, 060404 (2020).
- [16] P. Li, C. Wang, J. Zhang, S. Chen, D. Guo, W. Ji, and D. Zhong, Single-layer CrI_3 grown by molecular beam epitaxy, *Sci. Bull.* **65**, 1064 (2020).
- [17] G. Kresse and J. Hafner, Ab initio molecular dynamics for liquid metals, *Phys. Rev. B* **47**, 558 (1993).
- [18] G. Kresse and J. Furthmüller, Efficient iterative schemes for ab initio total-energy calculations using a plane-wave basis set, *Phys. Rev. B* **54**, 11169 (1996).
- [19] G. Kresse and D. Joubert, From ultrasoft pseudopotentials to the projector augmented-wave method, *Phys. Rev. B* **59**, 1758 (1999).
- [20] J. P. Perdew, K. Burke, and M. Ernzerhof, Generalized gradient approximation made simple, *Phys. Rev. Lett.* **77**, 3865 (1996).
- [21] S. L. Dudarev, G. A. Botton, S. Y. Savrasov, C. J. Humphreys, and A. P. Sutton, Electron-energy-loss spectra and the structural stability of nickel oxide: An LSDA+U study, *Phys. Rev. B* **57**, 1505 (1998).
- [22] H. J. Monkhorst and J. D. Pack, Special points for brillouin-zone integrations, *Phys. Rev. B* **13**, 5188 (1976).
- [23] S. Grimme, Semiempirical GGA-type density functional constructed with a long-range dispersion correction, *J. Comput. Chem.* **27**, 1787 (2006).
- [24] H. Li, Y.-K. Xu, K. Lai, and W.-B. Zhang, The enhanced ferromagnetism of single-layer CrX_3 ($\text{X}=\text{Br}$ and I) via van der waals engineering, *Phys. Chem. Chem. Phys.* **21**, 11949 (2019).
- [25] H. Li, Y.-K. Xu, Z.-P. Cheng, B.-G. He, and W.-B. Zhang, Spin-dependent schottky barriers and vacancy-induced spin-selective ohmic contacts in magnetic vdW heterostructures, *Phys. Chem. Chem. Phys.* **22**, 9460 (2020).
- [26] H. Ye, X. Wang, D. Bai, J. Zhang, X. Wu, G. P. Zhang, and J. Wang, Significant enhancement of magnetic anisotropy and conductivity in GaN/CrI_3 van der waals heterostructures via electrostatic doping, *Phys. Rev. B* **104**, 075433 (2021).
- [27] G. Henkelman, A. Arnaldsson, and H. Jónsson, A fast and robust algorithm for bader decomposition of charge density, *Comp. Mater. Sci.* **36**, 354 (2006).
- [28] L. Webster and J.-A. Yan, Strain-tunable magnetic anisotropy in monolayer CrCl_3 , CrBr_3 , and CrI_3 , *Phys. Rev. B* **98**, 144411 (2018).
- [29] Z. Wu, J. Yu, and S. Yuan, Strain-tunable magnetic and electronic properties of monolayer CrI_3 , *Phys. Chem. Chem. Phys.* **21**, 7750 (2019).
- [30] I. G. Rau, S. Baumann, S. Rusponi, F. Donati, S. Stepanow, L. Gragnaniello, J. Dreiser, C. Piamonteze, F. Nolting, S. Gangopadhyay, *et al.*, Reaching the magnetic anisotropy limit of a 3d metal atom, *Science* **344**, 988 (2014).
- [31] J. B. Goodenough, *Magnetism and the Chemical Bond* (Interscience-Wiley, New York, 1963).
- [32] J. Kim, K.-W. Kim, B. Kim, C.-J. Kang, D. Shin, S.-H. Lee, B.-C. Min, and N. Park, Exploitable magnetic anisotropy of the two-dimensional magnet CrI_3 , *Nano Lett.* **20**, 929 (2019).
- [33] T. Moriya, Anisotropic superexchange interaction and weak ferromagnetism, *Phys. Rev.* **120**, 91 (1960).
- [34] J. Liang, W. Wang, H. Du, A. Hallal, K. Garcia, M. Chshiev, A. Fert, and H. Yang, Very large Dzyaloshinskii-Moriya interaction in two-dimensional janus manganese dichalcogenides and its application to realize skyrmion states, *Phys. Rev. B* **101**, 184401 (2020).
- [35] X. Ma, G. Yu, C. Tang, X. Li, C. He, J. Shi, K. L. Wang, and X. Li, Interfacial dzyaloshinskii-moriya interaction: Effect of 5d band filling and correlation with spin mixing conductance, *Phys. Rev. Lett.* **120**, 157204 (2018).
- [36] X. Ma, G. Yu, C. Tang, X. Li, C. He, J. Shi, K. L. Wang, and X. Li, Interfacial Dzyaloshinskii-Moriya interaction: Effect of 5d band filling and correlation with spin mixing conductance, *Phys. Rev. Lett.* **120**, 157204 (2018).
- [37] J. Yuan, Y. Yang, Y. Cai, Y. Wu, Y. Chen, X. Yan, and L. Shen, Intrinsic skyrmions in monolayer Janus magnets, *Phys. Rev. B* **101**, 094420 (2020).
- [38] A. Fert and P. M. Levy, Role of anisotropic exchange interactions in determining the properties of spin-glasses, *Phys. Rev. Lett.* **44**, 1538 (1980).
- [39] L. M. Sandratskii, Insight into the Dzyaloshinskii-Moriya interaction through first-principles study of chiral magnetic structures, *Phys. Rev. B* **96**, 024450 (2017).
- [40] F. Zhang, X. Li, Y. Wu, X. Wang, J. Zhao, and W. Gao, Strong dzyaloshinskii-moriya interaction in monolayer CrI_3 on metal substrates, *Phys. Rev. B* **106**, L100407 (2022).